AMERICAN SOCIETY FOR MICROBIOLOGY | Journal of Virology®

PATHOGENESIS AND IMMUNITY

Heat Shock-Binding Protein 21 Regulates the Innate Immune Response to Viral Infection

Yan Xu,[a] Qiong Yang,[a] Binbin Xue,[a] Xintao Wang,[a] Renyun Tian,[a] Rilin Deng,[a] Shengwen Chen,[a] Xiaohong Wang,[a] Luoling Wang,[a] Cong Wang,[a] Jinwen Chen,[a] Ruina You,[a] Qian Liu,[a] Huiyi Li,[a] Jingjing Wang,[a] Xinran Li,[a] Shun Liu,[a] Di Yang,[a] Songqing Tang,[a] Haizhen Zhu[a,b]

[a]Institute of Pathogen Biology and Immunology of College of Biology, Hunan Provincial Key Laboratory of Medical Virology, State Key Laboratory of Chemo/Biosensing and Chemometrics, Hunan University, Changsha, China

[b]Research Center of Cancer Prevention and Treatment, Translational Medicine Research Center of Liver Cancer, Hunan Cancer Hospital, Changsha, China

ABSTRACT The induction of interferons (IFNs) plays an important role in the elimination of invading pathogens. Heat shock binding protein 21 (HBP21), first known as a molecular chaperone of HSP70, is involved in tumor development. Heat shock binding proteins have been shown to regulate diverse biological processes, such as cell cycle, kinetochore localization, transcription, and cilium formation. Their role in antimicrobial immunity remains unknown. Here, we found that HBP21 drives a positive feedback loop to promote IRF3-mediated IFN production triggered by viral infection. HBP21 deficiency significantly impaired the virus-induced production of IFN and resulted in greater susceptibility to viral infection both *in vitro* and *in vivo*. Mechanistically, HBP21 interacted with IRF3 and promoted the formation of a TBK1-IRF3 complex. Moreover, HBP21 abolished the interaction between PP2A and IRF3 to repress the dephosphorylation of IRF3. Analysis of HBP21 protein structure further confirmed that HBP21 promotes the activation of IRF3 by depressing the dephosphorylation of IRF3 by PP2A. Further study demonstrated that virus-induced phosphorylation of Ser85 and Ser153 of HBP21 itself is important for the phosphorylation and dimerization of IRF3. Our study identifies HBP21 as a new positive regulator of innate antiviral response, which adds novel insight into activation of IRF3 controlled by multiple networks that specify behavior of tumors and immunity.

IMPORTANCE The innate immune system is the first-line host defense against microbial pathogen invasion. The physiological functions of molecular chaperones, involving cell differentiation, migration, proliferation and inflammation, have been intensively studied. HBP21 as a molecular chaperone is critical for tumor development. Tumor is related to immunity. Whether HBP21 regulates immunity remains unknown. Here, we found that HBP21 promotes innate immunity response by dual regulation of IRF3. HBP21 interacts with IRF3 and promotes the formation of a TBK1-IRF3 complex. Moreover, HBP21 disturbs the interaction between PP2A and IRF3 to depress the dephosphorylation of IRF3. Analysis of HBP21 protein structure confirms that HBP21 promotes the activation of IRF3 by blocking the dephosphorylation of IRF3 by PP2A. Interestingly, virus-induced Ser85 and Ser153 phosphorylation of HBP21 is important for IRF3 activation. Our findings add to the known novel immunological functions of molecular chaperones and provide new insights into the regulation of innate immunity.

KEYWORDS HSP70, heat shock-binding protein 21, IRF3, molecular chaperone, PP2A, innate immunity, interferons, viral infection

We live in a world full of pathogens, and the human immune system, comprising the innate immune system and the adaptive immune system, fights against them to keep us healthy and disease-free. The innate immune system is the first-line host defense against viral infections, which is kicked off very early during virus infection,

Editor Bryan R. G. Williams, Hudson Institute of Medical Research

Address correspondence to Haizhen Zhu, zhuhaizhen69@yahoo.com.

The authors declare no conflict of interest.

Received 7 January 2022
Accepted 2 February 2022
Published 7 March 2022

whereas the adaptive immune system is dependent on the activation of the innate immune system (1).

Interferons (IFNs), divided into three groups (type I, type II, and type III), mediate a key innate immune response to a wide variety of viruses. All mammalian cells in the body can produce type I IFNs (IFN-α and IFN-β, etc.). There are many protein sensors, e.g., Toll-like receptors (TLRs), retinoic acid-inducible gene I (RIG-I)-like receptors (RLRs), NOD-like receptors (NLRs), and cyclic GMP-AMP synthase (cGAS), that detect the incoming virus particles, in the cytoplasm or inside specific cellular compartments (2–5). The protein sensors trigger activation of the main intracellular kinase TANK-binding kinase 1 (TBK1) and IκB kinase beta (IKKβ), leading to the induction of IFNs through interaction of the transcription factor interferon regulatory factor 3 (IRF3) (6–8). IFNs are secreted from virus-infected cells so that they can inhibit virus replication in infected cells, as well as protecting neighboring uninfected cells by inducing the expression of several hundred interferon-stimulated genes (ISGs) with antiviral efficiency (9, 10). ISGs can be directly induced by activated IRF3 as well, without any involvement of IFN (11–13).

IRF3, as a master transcription factor responsible for the induction of IFN, is fundamental for innate immunity. IRF3 is inactive in uninfected cells, and virus infection activates it by causing phosphorylation of its specific serine residue (14). Afterward, the phosphorylated IRF3 undergoes conformational changes and homodimerization, leading to its translocation to the nucleus and binding to p300/CBP, which ultimately leads to the early generation of IFN and the subsequent establishment of an antiviral state (15, 16). Therefore, the central aspect of IFN production relies on IRF3. IKKε and TBK1 are important components of the IRF3 signaling pathway (17). TBK1 and IKKβ are necessary but not sufficient to phosphorylate IRF3 (18). Other proteins are involved in IRF3 regulation of natural immunity. Protein arginine methyltransferase 6 (PRMT6), by blocking TBK1-IRF3 signaling, attenuates the ability of IRF3 in antiviral innate immunity (19). IRF1 augments the activation of IRF3 by blocking the interaction between IRF3 and PP2A to promote innate immunity (20).

Heat shock binding protein 21 (HBP21) contains three adjacent tetratricopeptide repeat (TPR) motifs and is the first known molecular chaperone of HSP70 (21). Heat shock binding proteins have been shown to regulate diverse biological processes, such as cell cycle, kinetochore localization, transcription, and cilium formation (22). These TPR motifs, each of which typically possesses a characteristic 34-amino-acid sequence conserved in evolution (23, 24), were originally identified in yeast cell division cycle proteins and successively found in a wide range of functionally irrelevant proteins, occurring in different organisms, including bacteria, plants, animals, and humans. Relying on the basic function of mediating protein-protein interaction, TPR-containing proteins, as scaffolds, are implicated in a variety of biological functions, such as chaperone, cell cycle, kinetochore localization, transcription and splicing, mitochondrial and endoplasmic reticulum (ER) protein transport, and cilium formation (25–27). Few studies on HBP21, especially in innate immunity, have been reported.

Here, we investigated the role of HBP21 in antiviral immunity. We found that HBP21 positively regulates the action of IRF3 in the innate immune response to viral infection *in vitro* and *in vivo*. Our findings reveal the dual regulation of IRF3 by HBP21. HBP21 stabilizes the formation of TBK1-IRF3 complex and promotes the activation of IRF3. Furthermore, HBP21 augments the activation of IRF3 by depressing the dephosphorylation of IRF3 by PP2A. Moreover, Ser85 and Ser153 phosphorylation for HBP21 is important for IRF3 activation. Our findings add to the known novel immunological functions of molecular chaperones and provide new insights into the regulation of innate immunity.

RESULTS

HBP21 promotes the innate immune response to viral infection *in vitro*. Tumor suppressors play an important role in immunity. The classical tumor suppressors PTEN (phosphatase and tensin homolog) and ARF (alternative reading frame) have been studied and found to play a critical role in antiviral innate immunity. As a tumor suppressor, the role of HBP21 in innate immunity is unknown. To investigate the role of HBP21 in innate

immunity, we measured the main genes participating in host antiviral defense by delivering or knocking down HBP21 in human HLCZ01 hepatocytes, which support the entire life cycle of hepatitis B virus (HBV) and HCV (28, 29). HBP21-overexpressing cells and HBP21-silenced cell lines were established (Fig. 1A and B). We used HBP21-silenced cell line 5 in subsequent experiments. MDA5 recognizes the high-molecular-weight (HMW) poly(I·C) and triggers the IFN pathway, while RIG-I can recognize HCV 3′-untranslated-region (UTR) RNA (30). Next, we used HMW poly(I·C) and HCV 3′-UTR RNA to stimulate HLCZ01 cells and measured the level of IFNs and ISGs. Exogenous HBP21 significantly enhanced the expression of type I IFN (IFN-β) and type III IFN (IL-28A) in HLCZ01 cells triggered by the synthetic RNA duplex poly(I·C) in a dose-dependent manner (Fig. 1C). ISG12a, an interferon-stimulated gene with antiviral properties (31), was also upregulated (Fig. 1C). Similarly, exogenous HBP21 in HLCZ01 cells augmented the expression of IFN-β, IL-28A, and ISG12a induced by HCV 3′-UTR RNA (Fig. 1D). Inversely, silencing of HBP21 significantly impaired the expression of IFN-β, IL-28A, and ISG12a induced by HMW poly(I·C) and HCV RNA 3′-UTR RNA (Fig. 1E and F). These data supported the idea that HBP21 promotes the innate immune response to nucleic acid mimics.

To further determine whether HBP21 plays a role in the innate immune response to viral infection, we used the RNA virus vesicular stomatitis virus (VSV) and the DNA virus herpes simplex virus (HSV) to stimulate the cells. Exogenous HBP21 in HLCZ01 cells augmented the expression of IFN-β, IL-28A, and ISG12a triggered by VSV or HSV infection at the indicated time points (Fig. 1G and H). As expected, knocking down HBP21 in HLCZ01 cells significantly impaired the expression of IFN-β, IL-28A, and ISG12a induced by VSV or HSV infection (Fig. 1I and J). Similarly, exogenous HBP21 in Huh7 cells augmented the expression of IFN-β, IL-28A, and ISG12a triggered by Newcastle disease virus (NDV) infection in the indicated time points (Fig. 1K). Viral infection usually alters the expression of genes, especially those involved in innate immunity. Indeed, VSV, HSV, and NDV infection induced the expression of HBP21 in the cells (Fig. 1L to N). Viral infection induces the production of type I and type III IFNs. IFNs recognize their receptors to activate the JAK/STAT pathway and induce the expression of ISGs, eliminating invading pathogens. IFN-α indeed induced the expression of HBP21 (Fig. 1O). To investigate whether the induction of HBP21 by viruses depends on the JAK/STAT pathway, we constructed a stable sg-IFNAR1 cell line using HLCZ01 cells. IFNAR1 was knocked out effectively in HLCZ01 cells (Fig. 1P). To ensure the efficiency of IFNAR1 knockout, we detected the phosphorylation of STAT1 and ISG15 with IFN-α treatment. Phosphorylation of STAT1 and ISG15 was attenuated in sg-IFNAR1 cells compared to the control cells (Fig. 1P). Furthermore, knockout of IFNAR1 significantly decreased the level of HBP21 in HLCZ01 cells with IFN-α treatment (Fig. 1P). All the data supported the idea that HBP21 promotes the innate immune response to viral infection and the induction of HBP21 depends on the IFN/JAK/STAT signaling pathway.

Pivotal role of HBP21 in the antiviral response *in vivo*. We constructed HBP21-deficient mice by using a CRISPR/Cas9 system to explore the function of HBP21 in innate immunity *in vivo*. We provide a diagram showing the murine HBP21 allele (Fig. 2A). We observed a prospective knockout effect in different tissues from HBP21$^{-/-}$ or wild-type mice through Western blotting (Fig. 2B). The induction of IFN-β by poly(I·C) was significantly decreased in peritoneal marrow derived macrophages (PMDMs) from HBP21$^{-/-}$ mice compared to PMDMs from wild-type mice (Fig. 2C). Similarly, IFN-β was markedly reduced in HBP21$^{-/-}$ PMDMs compared with PMDMs from wild-type mice upon VSV or HSV infection (Fig. 2D and E). Consistently, the level of IFN-β in sera was severely decreased in HBP21 deletion mice compared with wild-type mice upon VSV infection (Fig. 2F). We also compared the survival rates of HBP21-wild-type and HBP21 deletion mice following inoculation of VSV. HBP21 deletion mice were more susceptible to VSV-triggered mortality than their wild-type counterparts (Fig. 2G). The expression of IFN-β was severely impaired in various organs of HBP21 deletion mice compared with the wild-type mice upon VSV infection (Fig. 2H). Consistently, the content of VSV was markedly increased in various organs of HBP21 deletion mice compared with the wild-type mice (Fig. 2I). As expected, there was serious inflammation in the lungs and livers of HBP21-deficient mice after VSV

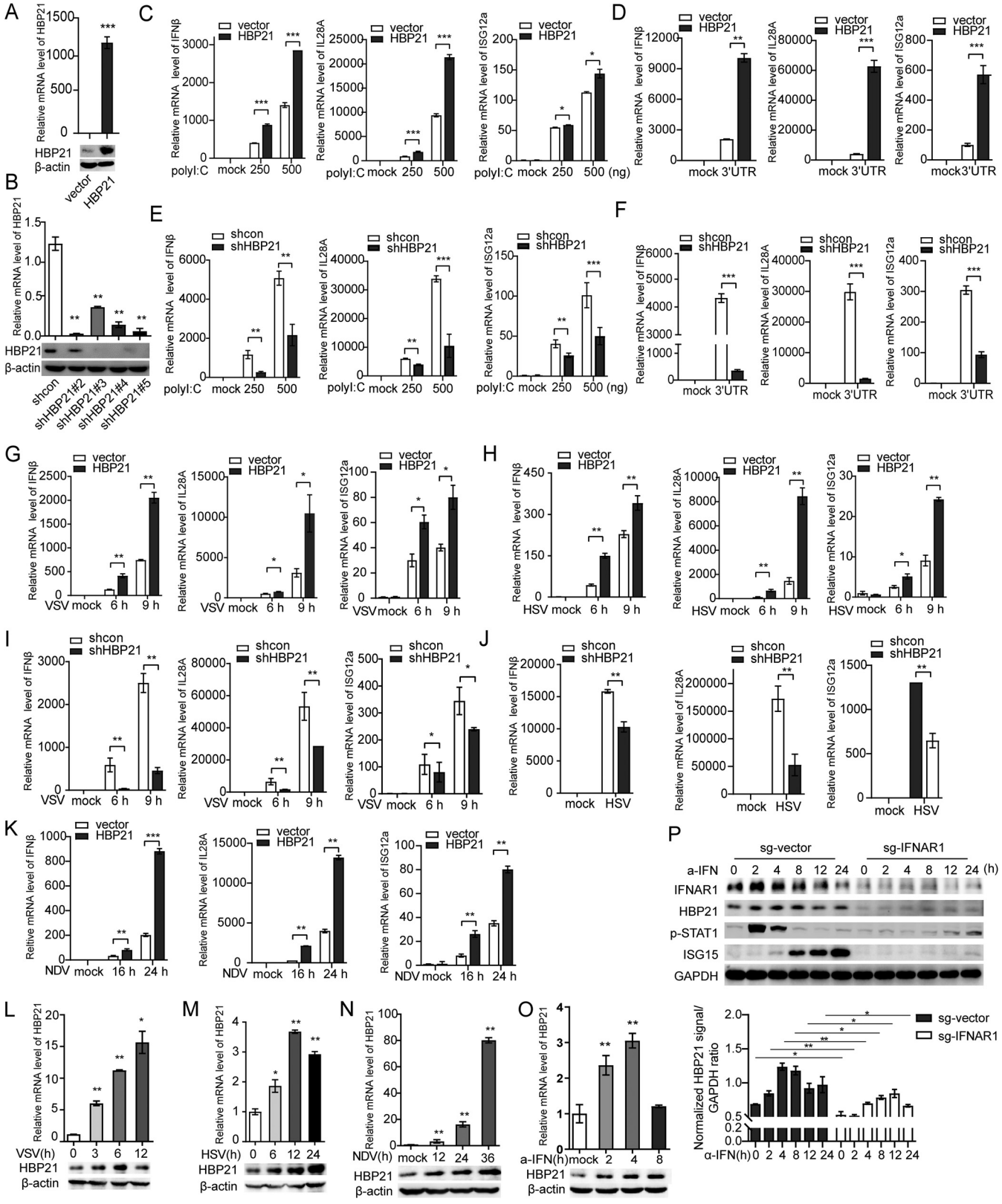

FIG 1 HBP21 promotes the innate immune response to viral infection *in vitro*. (A) Real-time PCR analysis of HBP21 from HLCZ01 cells transfected by p3XFlag-HBP21 was performed, and immunoblotting assays were performed for HBP21 and β-actin antibodies. (B) HLCZ01 cells were transfected with control or specific shRNA targeting HBP21, which was treated with puromycin (2 μg/mL) for 1 month. HBP21 mRNA level was examined by reverse transcription-PCR (RT-PCR) and normalized with GAPDH. Immunoblot analysis of HBP21 and β-actin in the HBP21-silenced HLCZ01 cells was performed. (C to F) HLCZ01 cells transfected with pFlag-HBP21 or empty vector or HBP21-silenced HLCZ01 cells were treated with poly(I·C) at the indicated doses or

(Continued on next page)

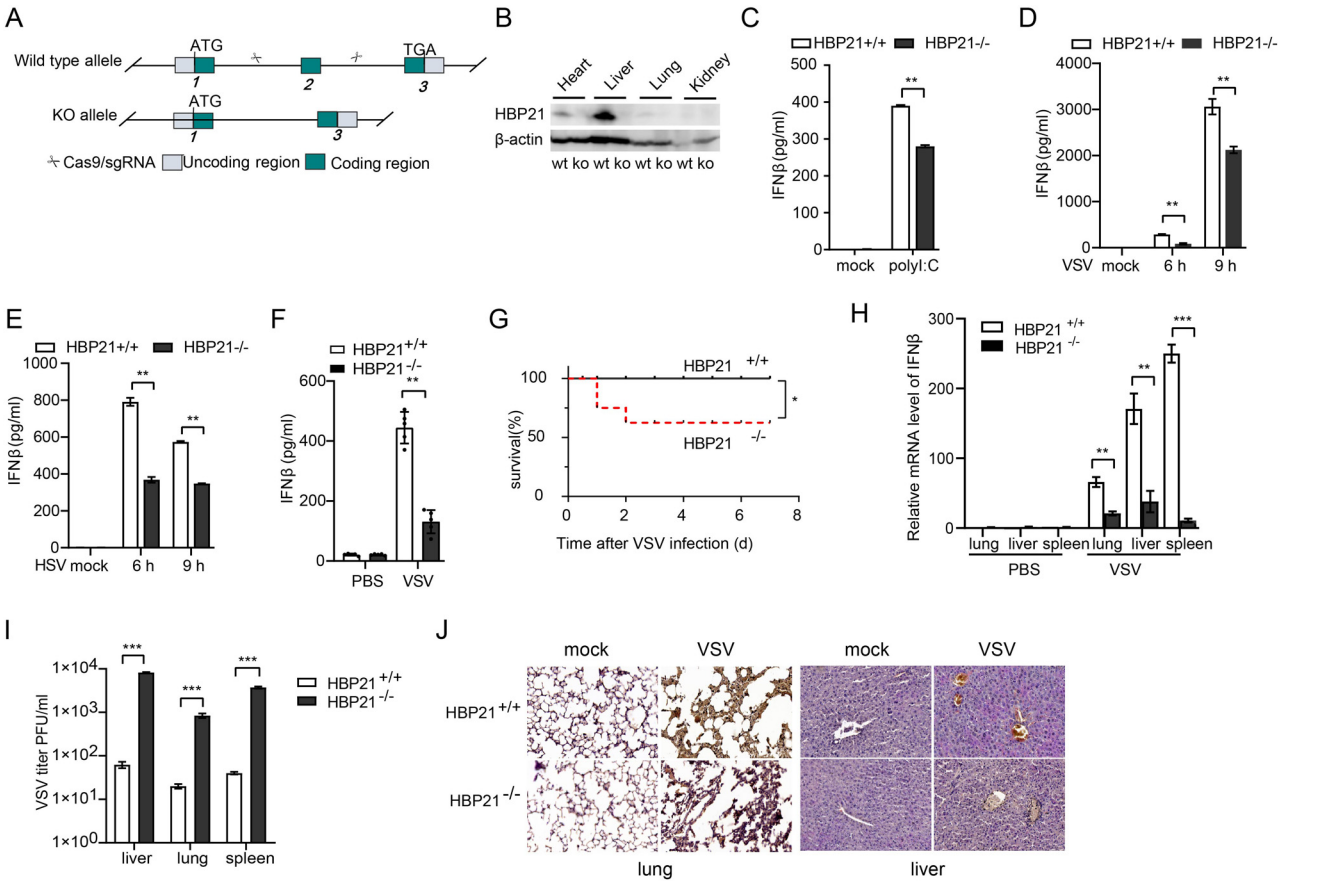

FIG 2 Pivotal role of HBP21 in the antiviral response *in vivo*. (A) CRISPR-Cas9 technology was used to edit the HBP21 gene in animal models, and the schematic diagram shows the murine HBP21 allele and the positions of single guide RNA (sgRNA). (B) Immunoblot analysis of HBP21 and β-actin from different tissues to identify the knockout effect. (C) ELISA of IFN-β in the culture medium of HBP21$^{+/+}$ and HBP21$^{-/-}$ macrophages transfected with 500 ng of poly(I·C) for 6 h. (D and E) ELISA of IFN-β in the supernatant of HBP21$^{+/+}$ and HBP21$^{-/-}$ macrophages with or without VSV (MOI = 1) or HSV (MOI = 1) infection for the indicated times. (F) ELISA of IFN-β in sera from wild-type (WT) mice (n = 5) and HBP21 knockout mice (n = 5) infected intraperitoneally for 18 h with VSV (1×10^7 PFU/g body weight). Each symbol represents an individual mouse, and small horizontal lines indicate the means. (G) Survival (Kaplan-Meier curve) of wild-type mice (n = 8) and HBP21$^{-/-}$ mice (n = 8) infected intraperitoneally with a high dose of VSV (1.5×10^7 PFU/g body weight) and monitored for 7 days. (H) The level of IFN-β mRNA was quantified in the lungs, livers, and spleens from wild-type mice (n = 3) and HBP21$^{-/-}$ mice (n = 3) after intraperitoneal infection with VSV (1×10^7 PFU/g body weight) for 18 h or not. (I) Plaque assay of VSV in lungs, livers, and spleens of wild-type mice (n = 3) and HBP21$^{-/-}$ mice (n = 3) after intraperitoneal infection with VSV (1×10^7 PFU/g body weight) for 18 h. (J) H&E staining of the lung and liver sections from WT mice or HBP21$^{-/-}$ mice 18 h after infection with VSV (as for panel D). *, $P < 0.5$, **, $P < 0.01$; ***, $P < 0.001$ (unpaired t test [F] or log-rank test [G]; means and SD in panels C, D, E, H, and I). Data are representative of two or three experiments.

infection (Fig. 2J). Together, these data supported the idea that HBP21 is critical for the antiviral innate immune response *in vivo*.

HBP21 regulates IRF3-mediated signaling axis and suppresses viral infection. Both the transcriptional activation of the IFN-β promoter and that of the NF-κB promoter trigger the induction of IFN-β (17). Ectopic expression of HBP21 enhanced the activation of IFN promoter upon VSV infection (Fig. 3A). In parallel experiments, the activity of NF-κB promoter was unaffected by HBP21 (Fig. 3B). IRF3 and IRF7 are responsible for the induction of IFN-α/β (32). Ectopic expression of HBP21 enhanced the IRF3-mediated

FIG 1 Legend (Continued)
200 ng of 3′ UTR for 9 h. The levels of IFN-β, IL-28A, and ISG12a mRNA were examined by RT-PCR and normalized to GAPDH. (G to J) HLCZ01 cells transfected with pFlag-HBP21 or empty vector and HBP21-silenced HLCZ01 cells were infected with VSV (multiplicity of infection MOI = 1) for the indicated times or HSV (MOI = 1) for 9 h. The levels of IFN-β, IL-28A, and ISG12a mRNA were examined by RT-PCR and normalized to GAPDH. (K) Huh7 cells transfected with pFlag-HBP21 or empty vector were infected with NDV (MOI = 0.04) for the indicated times. The levels of IFN-β, IL-28A, and ISG12a mRNA were examined by RT-PCR and normalized to GAPDH. (L to O) Immunoblot analysis and RT-PCR analysis of HBP21 in HLCZ01 cells upon VSV (MOI = 1), HSV (MOI = 0.5), or NDV (MOI = 0.01) infection or with α-IFN (100 U/mL) treatment for the indicated times. (P) Immunoblot analysis of the indicated proteins in HLCZ01-sg-vector and HLCZ01-sg-IFNAR1 stable cell lines treated with IFN-α (100 U/mL) for the indicated times. Values are means and standard deviations (SD). *, $P < 0.05$; **, $P < 0.01$; ***, $P < 0.001$. Data are representative of three experiments.

activation of IFN-β promoter while it did not affect IRF7-mediated activation of the IFN-β promoter (Fig. 3C). Phosphorylation of IRF3 was enhanced in HBP21-overexpressing HLCZ01 cells and remarkably attenuated in HBP21-silenced cells, but other indicated signal proteins involving the IFN signaling pathway had no change (Fig. 3D). Macrophages from HBP21$^{-/-}$ mice showed a significant reduction of both phosphorylated IRF3 and its downstream STAT1 activation upon VSV infection, compared to wild-type littermate (Fig. 3E). As well, phosphorylation of IRF3 was enhanced in HBP21-overexpressing Huh7 cells upon NDV infection (Fig. 3F). Similarly, phosphorylated IRF3 was augmented or impaired in HBP21-overexpressing or HBP21-silenced HLCZ01 cells upon HSV infection, respectively (Fig. 3G and H). The phosphorylated IRF3 undergoes homodimerization and is translocated into the nucleus, causing the transcription of IFN genes (4). In parallel experiments, exogenous HBP21 or knocking down of HBP21 enhanced or attenuated the phosphorylation and dimerization of IRF3 triggered by VSV in HLCZ01 cells, respectively (Fig. 3I). To prove the rigor of the mechanism, we examined the effect of HBP21 on IRF3 entry into the nucleus. As expected, the import of IRF3 from the cytoplasm into the nucleus was significantly augmented in HBP21-overexpressing cells upon VSV infection (Fig. 3J). These data demonstrate the critical role of HBP21 in IRF3-mediated innate immunity.

Since HBP21 is involved in IRF3-dependent innate immune response to viral infection, we next investigated whether HBP21 contributes to antiviral responses during viral infection. In our previous study, HCV infection was found to induce the expression of IFN in HLCZ01 cells (33). We found that protein 3 (NS3) of HCV was lower in HBP21-overexpressing HLCZ01 cells than in the control cells. As expected, NS3 levels were higher in HBP21-silenced HLCZ01 cells than in control cells (Fig. 3K and L). Similarly, HBP21 inhibits the replication of VSV and HSV (Fig. 3M and N), and the replication of VSV or HSV encoding a green fluorescent protein (GFP) reporter (VSV-GFP and HSV-GFP) was enhanced, as indicated by enhanced GFP expression in HBP21-silenced cells (Fig. 3O). We also confirmed that HBP21 did not affect the IFN-α-activated downstream signaling pathway (Fig. 3P and Q). These data support the idea that HBP21 promotes IRF3-mediated innate immunity and possesses the biological function of antiviral activity.

HBP21 targets and interacts with IRF3. To determine the molecular mechanism of HBP21 in enhancing IFN signaling pathway, we investigated whether HBP21 targets IRF3 or its upstream steps. Overexpression of HBP21 markedly enhanced the activation of IFN-β reporter by upstream activators (RIG-I, MDA5, MAVS, and TBK1) and the constitutive active phosphorylation mimetic IRF3-5D (34) (Fig. 4A). The IFN-β reporter activity triggered by the activators (cGAS and STING) was considerably augmented in HBP21-overexpressing cells (Fig. 4B). The data show that HBP21 is involved in the innate immunity induced by either RNA virus or DNA virus. Additionally, HBP21 does not affect the phosphorylation of TBK1. These data indicated that HBP21 may exert its function at IRF3. HBP21 indeed interacted with IRF3, while no interaction between HBP21 and TBK1 was observed (Fig. 4C and D). The interaction between HBP21 and endogenous IRF3 was confirmed in HEK-293T cells (Fig. 4E). Furthermore, a strong association of HBP21 and IRF3 was enhanced in HLCZ01 cells upon VSV or HSV infection (Fig. 4F). Next, to better understand the molecular mechanism of HBP21-mediated IRF3 function, we constructed a series of truncations of IRF3. IRF3 contains a conserved DNA binding domain (DBD), an IRF association domain (IAD), and a C-terminal autoinhibition element (AIE) (35). IAD IRF3, which contains phosphorylation sites known to be important for IRF3 dimerization (18), interacted with HBP21 (Fig. 4G and H). The truncation experiments with HBP21 revealed that the domain of HBP21 from amino acid (aa) 50 to 189 was the key domain for the HBP21-IRF3 interaction (Fig. 4I and J). These data supported the idea that HBP21 targets IRF3 and the aa 50–189 domain of HBP21 is important for its interaction with the IAD domain of IRF3.

HBP21 promotes the formation of the TBK1-IRF3 complex. The TBK1-IRF3 signaling cascade is a common pathway that is activated by the adaptor proteins MAVS and STING (36). Our data demonstrated that HBP21 promotes both MAVS- and STING-induced IFN transcription, indicating that HBP21 may target the TBK1 and IRF3 signaling complex. As mentioned above, HBP21 is composed of three adjacent TPR motifs. TPR domain proteins are involved in a wide range of cellular processes and play a crucial role in understanding

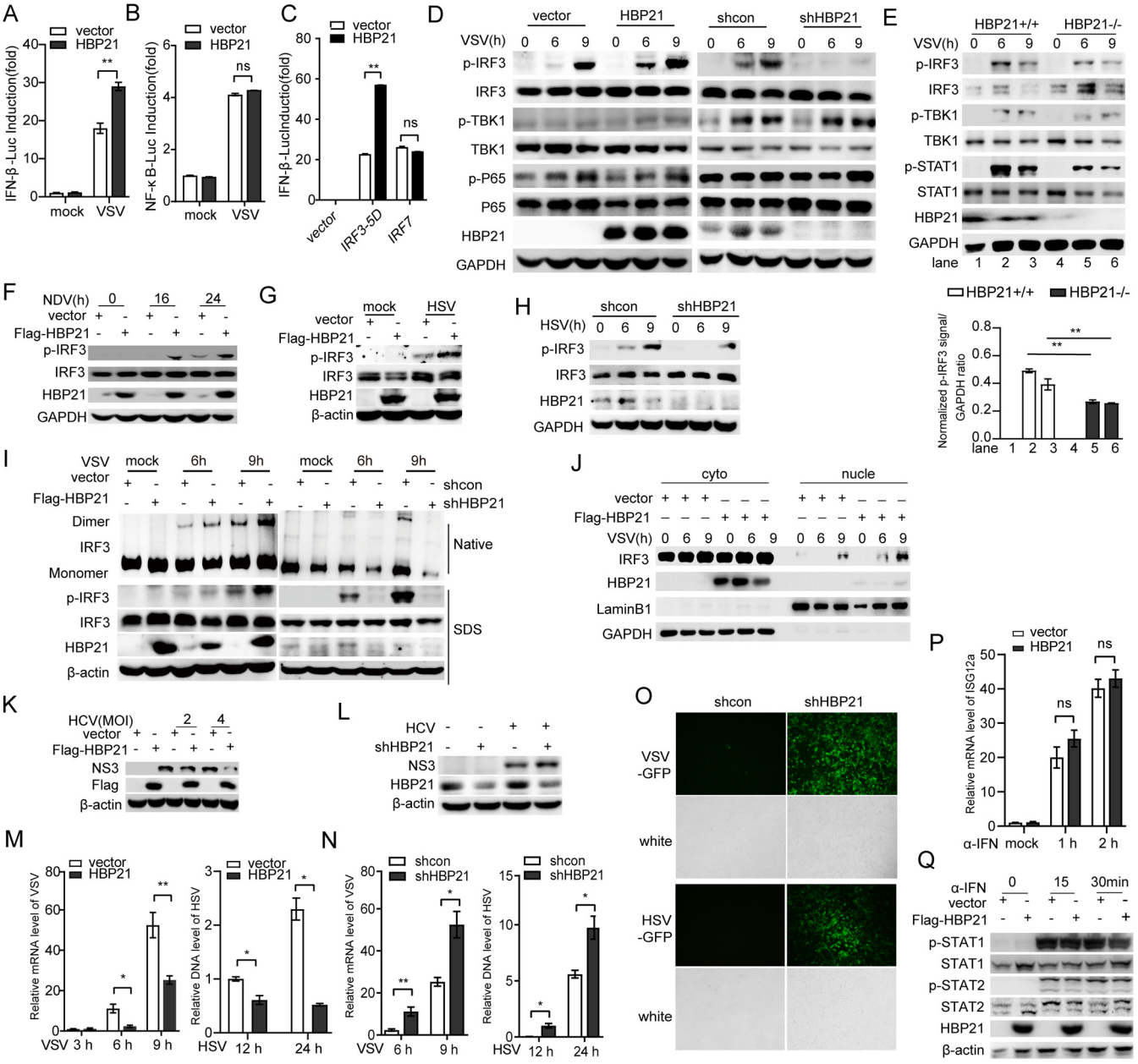

FIG 3 HBP21 regulates IRF3-mediated signaling axis and suppresses viral infection. (A) Dual luciferase analysis of the activity of the IFN-β promoter in HEK293T cells cotransfected with encoding HBP21 and IFN-β promoter plasmids upon VSV (MOI = 1) infection for 6 h. (B) Dual luciferase analysis of the activity of NF-κB promoter in HEK293T cells cotransfected with pFlag-HBP21 and NF-κB-luc plasmid upon VSV (MOI = 1) infection for 6 h. (C) Dual luciferase analysis of the activity of the IFN promoter in HEK293T cells cotransfected with pFlag-HBP21, IFN-luc plasmid, and p3XFlag-IRF3-5D or p3XFlag-IRF7. (D) HLCZ01 cells transfected with pFlag-HBP21 or empty vector or HBP21-silenced HLCZ01 cells were infected with VSV (MOI = 1) for the indicated times. Immunoblotting assays were performed with the indicated antibodies. (E) HBP21$^{+/+}$ and HBP21$^{-/-}$ macrophages were infected with VSV (MOI = 1) for the indicated times. Immunoblotting assays were performed with the indicated antibodies. (F) Huh7 cells transfected with pFlag-HBP21 or empty vector were infected with NDV (MOI = 0.04) for the indicated times. Immunoblotting assays were performed with the indicated antibodies. (G) Immunoblot analysis of p-IRF3 (S396) in HLCZ01 cells transfected with pFlag-HBP21 or empty vector followed with HSV (MOI = 1) infection for 9 h. (H) Immunoblot analysis of p-IRF3 (S396) in HBP21-silenced HLCZ01 or control cells upon HSV (MOI = 1) infection for the indicated times. (I) Immunoblot analyses of IRF3 in dimer or monomer form, IRF3 phosphorylated at Ser396 [p-IRF3(S396)], total IRF3, and HBP21 were performed by native PAGE or SDS-PAGE in HLCZ01 cells transfected with pFlag-HBP21 or HBP21-silenced HLCZ01 cells with VSV infection. (J) Immunoblot analysis of nucleus-cytoplasm extraction of HBP21-overexpressing HLCZ01 cells upon VSV (MOI = 1) infection. (K and L) HLCZ01 cells were transfected with pFlag-HBP21 or empty vector for 24 h and then infected with HCV (MOI = 2 and 4) for 48 h. The shHBP21-stable HLCZ01 or shVector HLCZ01 cells were infected with HCV (MOI = 4) for 72 h. Immunoblot analysis of nonstructural protein 3 (NS3) of HCV was performed. (M and N) Real time-PCR analysis of VSV in HBP21-overexpressing HLCZ01 cells or HBP21-silenced HLCZ01 cells with VSV (MOI = 1) infection. PCR analysis of HSV in HBP21-overexpressing HLCZ01 cells or HBP21-silenced HLCZ01 cells with HSV (MOI = 0.5) infection. (O) The stable HBP21-silenced HLCZ01 cells and control cells were infected for 24 h with VSV-GFP or HSV-GFP (MOI = 0.1). Bars, 100 μm. (P and Q) HLCZ01 cells were transfected with pFlag-HBP21 or empty vector and then treated with IFN-α (100 U/mL) for the indicated times. Real-time PCR analysis of ISG12a. Immunoblot analysis of indicated antibodies. Data are representative of three independent experiments (means and SD are shown in panels A, B, C, M, N, and P).

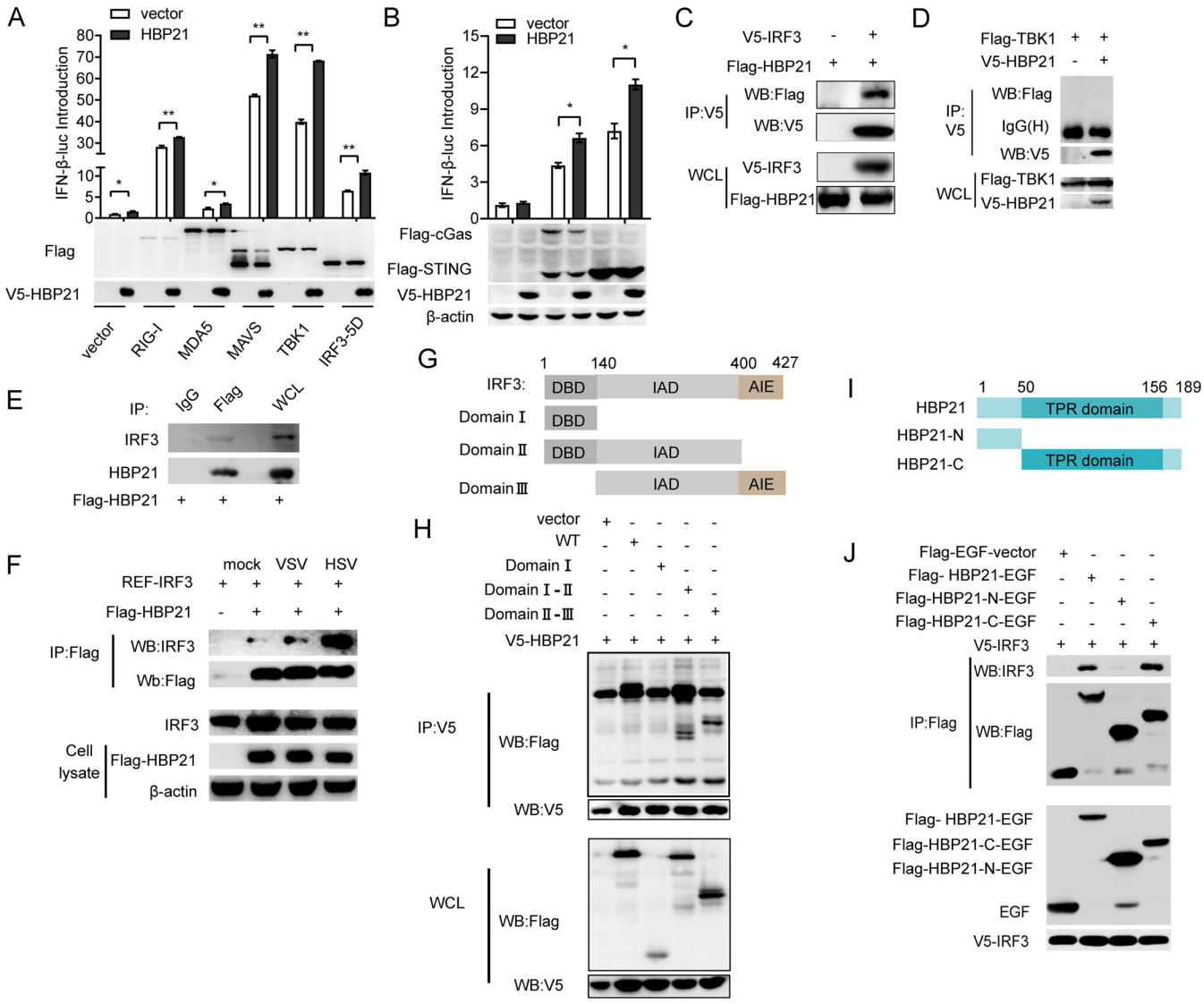

FIG 4 HBP21 targets and interacts with IRF3. (A) Dual luciferase assay (top) and immunoblot analysis (bottom) of HEK293T cells transfected with the IFN promoter and RIG-I-N, MDA5, MAVS, TBK1, or IRF3-5D and HBP21 or empty vector. (B) HEK293T cells were transfected with the IFN promoter and 0.5 μg STING, 0.5 μg cGAS or 1 μg STING, and HBP21. Dual luciferase assay (top) and immunoblot analysis (bottom) were performed. (C and D) HEK293T cells were cotransfected with pcDNA3.1a-IRF3 and p3XFlag-HBP21 or with p3XFlag-TBK1 and pcDNA3.1a-HBP21, and immunoprecipitation and Western blotting were performed with the indicated antibodies. (E) HEK293T cells were transfected with pFlag-HBP21, and immunoprecipitation and Western blotting were performed with the indicated antibodies. (F) HLCZ01 cells were cotransfected with pREF-IRF3 and pFlag-HBP21, followed by VSV (MOI = 1) or HSV (MOI = 1) infection for 9 h. Then, immunoprecipitation and Western blotting were performed with the indicated antibodies. (G) Schematic illustration of IRF3 truncation. DBD, DNA binding domain; IAD, IRF3 association domain; AIE, C-terminal autoinhibition element. (H) HEK293T cells were cotransfected with the plasmid encoding IRF3 or the indicated domain and HBP21 for 36 h. Co-IP and immunoblotting were performed with the indicated antibodies. (I) Schematic illustration of IRF3 truncation. The carboxyl-terminal region is aa 1 to 50; the N-terminal region is aa 50 to 189. (J) HEK293T cells were cotransfected with plasmid encoding HBP21 or the indicated domain and full-length pcDNA3.1a-IRF3 for 48 h. Co-IP and immunoblotting were performed with the indicated antibodies. Data are representative of three independent experiments.

protein-protein interaction assembly (37). Therefore, we hypothesized that HBP21 may affect the interaction between TBK1 and IRF3. To test this conjecture, we cotransfected plasmids encoding TBK1 and HBP21 into HEK293T cells. Exogenous HBP21 enhanced the interaction between IRF3 and exogenous TBK1 (Fig. 5A). Our above data showed that HBP21 interacts with IRF3 and enhances its phosphorylation and that TBK1 activation was unchanged while IRF3 phosphorylation was decreased in VSV-infected HBP21-deficient PMDMs. Endogenous TBK1-IRF3 interaction was enhanced in HBP21-overexpressing HLCZ01 cells compared to control cells upon VSV or HSV infection (Fig. 5B and C). Inversely, the TBK1-IRF3 interaction was markedly impaired in HBP21-silenced cells compared to control cells upon VSV infection (Fig. 5D). These data echoed the observation that the TPR structure of HBP21 as a scaffold can

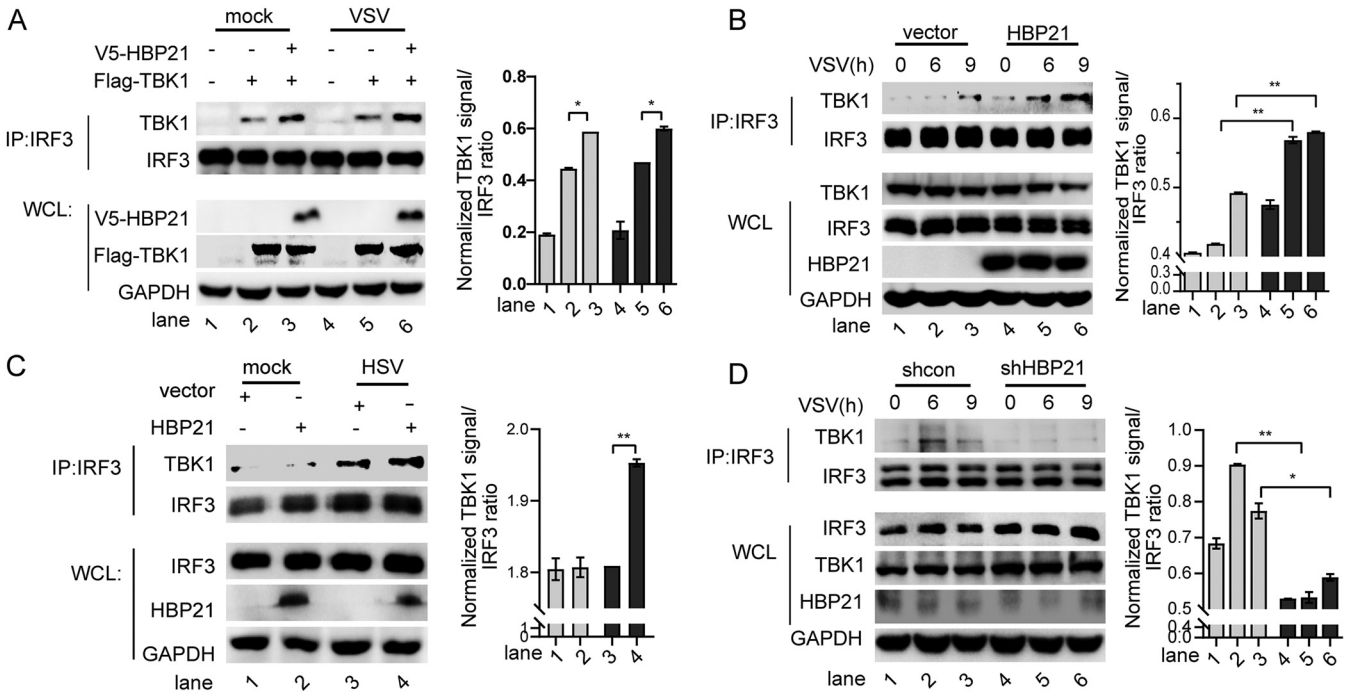

FIG 5 HBP21 promotes the formation of TBK1-IRF3 complex. (A) HEK293T cells were cotransfected with p3XFlag-TBK1 and pcDNA3.1a-HBP21 for 36 h, followed by VSV infection for 6 h. Immunoprecipitation and Western blotting were performed with the indicated antibodies. (B and C) HLCZ01 cells transfected with p3XFlag-HBP21 were infected with VSV (MOI = 1) or HSV (MOI = 1). Immunoprecipitation was performed with the indicated antibodies. (D) HBP21-silenced HLCZ01 cells were infected with VSV (MOI = 1) for the indicated times. Immunoprecipitation was performed with the indicated antibodies. Data are representative of three independent experiments.

regulate protein-protein interaction. Taken together, all the data supported the idea that HBP21 promotes the antiviral innate immune response by targeting the TBK1-IRF3 signaling complex.

The phosphorylation of Ser85 and Ser153 in HBP21 is necessary for the activation of IRF3 during viral infection. The TPR consensus sequence is highly conserved at key positions vital for both structure and function. HBP21 protein consists of 189 amino acids, of which aa 49 to 156 are TPR structures. To make the potentially conserved sites clear, we compared the amino acid sequences of HBP21 proteins from 9 different species of mammals (Fig. 6A). Subsequently, HBP21 was predicted by UniProt online software based on the sequence alignment. We found that a strong signal of phosphorylation modification of HBP21 was predicted through comprehensive resources for the study of protein posttranslational modifications (PTMs) in humans, mice, and rats in the UniProt software. Coincidentally, we found that two highly conserved serine sites are located at amino acid positions 85 and 153 of HBP21. Serine phosphorylation is very classical. Therefore, we tested whether HBP21 may be phosphorylated during viral infection. To test this hypothesis, we performed a phosphorylation assay and found that wild-type HBP21 was phosphorylated, but not the serine mutant HBP21 (Fig. 6B and C). These data demonstrated that virus infection triggers the phosphorylation of HBP21.

Next, we speculated that the phosphorylation of HBP21 plays an important role in its function. To test this assumption, we individually replaced each conserved serine residue of HBP21 with alanine (phosphorylation-deficient mutant) or aspartic acid (phosphorylation mimic mutant) and also created the respective double mutants. We introduced each of these mutants into HLCZ01 cells to assess their ability to activate the IFN-β promoter. Excitingly, the effects of substitutions S85A and S153A on the activation of IFN-β or IRF3 (at Ser396) were much lower than the wild-type HBP21 (Fig. 6D and E). Consistent with these observations, the production of IFN-β and the activation of IRF3 were enhanced in S85D or S153D HBP21-expressing HLCZ01 cells (Fig. 6F and G). Upon VSV infection, wild-type HBP21 but not the mutant reversed the impaired

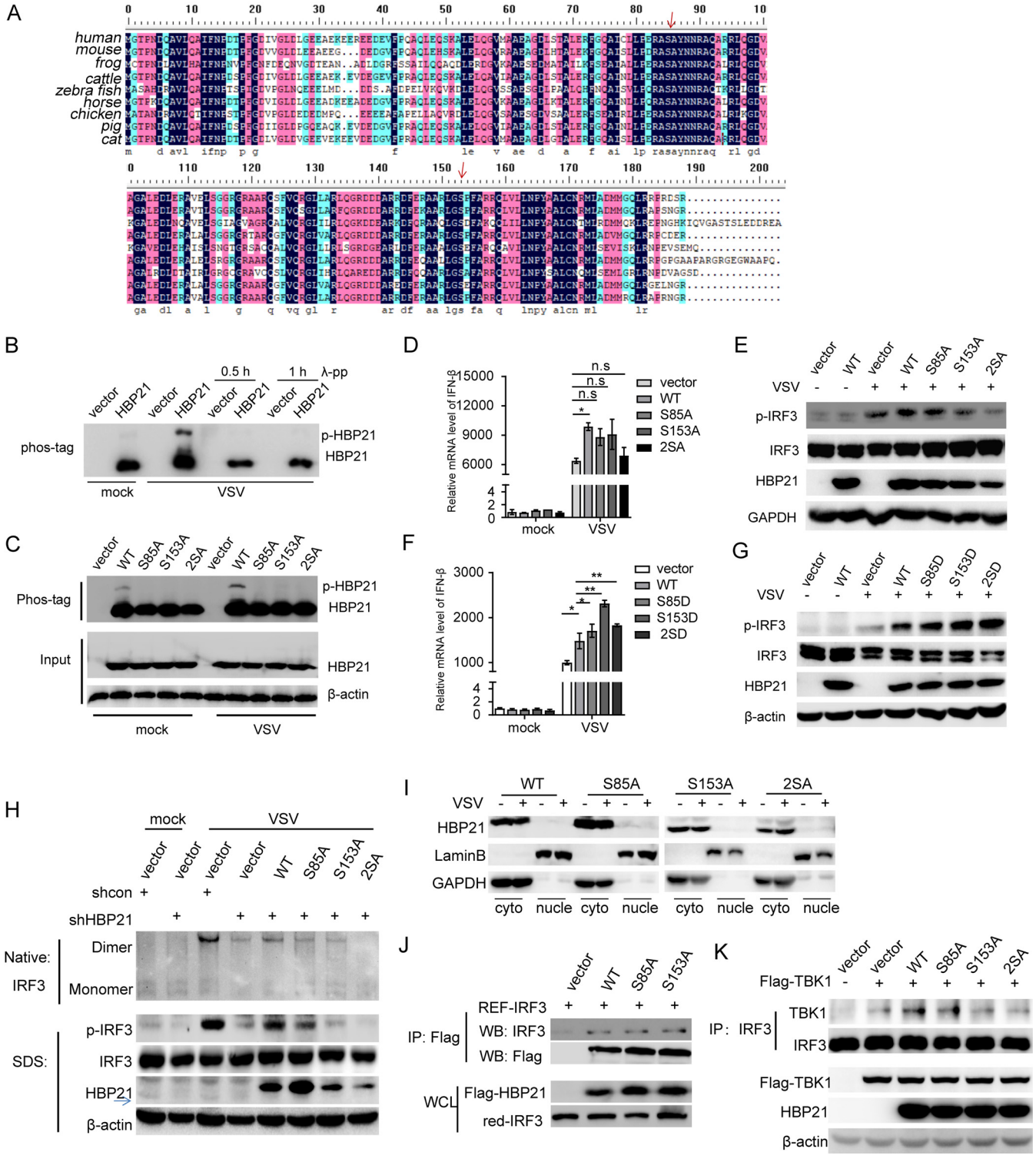

FIG 6 The phosphorylation of HBP21 at Ser85 and Ser153 is important for the activation of IRF3 during viral infection. (A) Alignment of HBP21 homologous protein was produced by the DNAMAN (7.0) program. (B) HEK293T cells were transfected with the plasmid encoding HBP21 for 24 h and then infected with VSV (MOI = 1) for 6 h. The protein was isolated and treated with phosphatase 37°C for 0.5 or 1 h, and immunoblotting of SDS-PAGE (Phos-tag [100 μM], $MnCl_2$ [200 μM]) of HBP21 was performed. (C) Immunoblot analysis of HBP21 in HLCZ01 cells transfected with the plasmid encoding wild-type HBP21 or alanine mutant HBP21 for 24 h, following treatment as for panel B. (D to G) HLCZ01 cells were transfected with the plasmid encoding wild-type HBP21 or alanine or aspartic mutant HBP21 for 36 h and then infected with VSV (MOI = 1) for 6 h. IFN-β mRNA level and phosphorylation of IRF3 at Ser396 were detected by real-time PCR and Western blotting, respectively. (H) HBP21-silenced cells or control cells were transfected by the plasmid encoding wild-type HBP21 or alanine mutant HBP21 and then infected with VSV (MOI = 1) for 9 h. Immunoblot analysis of IRF3 in dimer or monomer form (top) or phosphorylation of IRF3 at Ser396, total IRF3 and HBP21 (bottom) in the cells with VSV infection for 6 and 9 h. (I) HLCZ01 cells transfected with

(Continued on next page)

phosphorylation (at Ser396) and dimerization of IRF3 caused by the knockdown of HBP21 (Fig. 6H). These results suggested that the phosphorylation of Ser85 and Ser153 in HBP21 is important for the activation of IRF3.

How does the phosphorylation of HBP21 affect the activation of IRF3? Phosphorylation modification may regulate the localization of the protein and then affect the function of the protein. However, a change of HBP21 localization was not observed (Fig. 6I). Moreover, the interaction between mutated HBP21 and IRF3 was not affected compared to wild-type HBP21 (Fig. 6J). Our above data showed that HBP21 regulates the TBK1-IRF3 complex and interacts with IRF3. Whether phosphorylation of HBP21 is involved in the process is unknown. To test our conjecture, intact or phosphorylation-deficient mutant HBP21 and TBK1 were cotransfected into HEK293T cells. HBP21 but not mutant HBP21 promoted TBK1-IRF3 interaction (Fig. 6K). Taken together, these data demonstrated that the phosphorylation of Ser85 and Ser153 of HBP21 is necessary for the activation of IRF3 and the formation of TBK1-IRF3 complex.

HBP21 blocks the interaction between PP2A and IRF3 to promote the innate immune response to viral infection. The TPR domain is a known protein-protein interaction motif that interacts with HSP70 and HSP90 (38). In addition, HSP90 interacts with the isolated TPR domain from protein phosphatase 5 (PP5) (39). PP5 uniquely comprises a regulatory N-terminal TPR domain fused to a C-terminal phosphatase catalytic domain, and the active site of the phosphatase catalytic domain is blocked by the TPR domain (40). The phosphatase catalytic domain is a conserved structural domain in members of the phosphoprotein phosphatases family, including PP1, PP2A, PP2B, PP4, PP5, PP6, and PP7. It is reported that PP2A is a phosphatase that targets IRF3 (20, 41). Taking these data together, we determined whether HBP21 containing a TPR domain inhibits the function of PP2A on IRF3. First, we analyzed the structure of PP2A, HBP21, and PP5, respectively, with the online software AlphaFold (42). We found that PP5 was like a combination of HBP21 and PP2A according to structure analysis (Fig. 7A). The data are consistent with the results summarized by Shi (43). We therefore directly investigated whether HBP21 abolishes the inhibition of innate immunity by PP2A. Overexpression of HBP21 reversed the reduction of IFN-β production by PP2A upon VSV infection (Fig. 7B), while knockdown of HBP21 further strengthened the inhibition of IFN production by PP2A upon VSV infection (Fig. 7C). Consistent with our assumption, overexpression of HBP21 impaired the ability of PP2A to suppress the activation of phosphorylated IRF3 (Fig. 7D). Ectopic expression of HBP21 further augmented the activation of phosphorylated IRF3 and the production of IFN-β in PP2A-silenced cells upon viral infection (Fig. 7E and F). These data supported that HBP21 inhibits the effect of PP2A on innate immunity. It has been reported that HBP21 inhibits the interaction between HSP70 and Bax (44), so we wanted to know whether HBP21 affects interaction between IRF3 and PP2A. Interestingly, overexpression of HBP21 abolished the interaction between PP2A and IRF3 in a dose-dependent manner (Fig. 7G), suggesting that HBP21 disturbs the interaction between PP2A and IRF3 through competing interaction with IRF3. Knockdown of HBP21 augmented the endogenous PP2A and IRF3 interaction (Fig. 7H). No obvious difference of the activity of IFN-β promoter was found in PP2A-silenced and HBP21-overexpressing cells compared with PP2A-silenced cells (Fig. 7I). All the data suggested that HBP21 abolishes the IRF3-PP2A interaction through competing interaction with IRF3 and subsequently augments the activation of IRF3, thereby promoting the innate immune response.

Finally, we established a schematic model for the dual regulation of IRF3 by HBP21 (Fig. 8). HBP21 is induced by viral infection. Upon virus infection, HBP21 is phosphorylated at S85 and S153. HBP21 enhances the formation of the TBK1-IRF3 complex and subsequently phosphorylates IRF3 at S396. Moreover, HBP21 promotes the activation of IRF3 by depressing

FIG 6 Legend (Continued)
the plasmid encoding wild-type HBP21 or vector alanine mutant HBP21 were infected with VSV (MOI = 1) for 24 h, followed by nucleus-cytoplasm extraction. Immunoblot analysis was performed. (J) HEK293T cells were cotransfected with the plasmid encoding IRF3 and the plasmid encoding wild-type HBP21 or alanine mutant HBP21 for 36 h. Immunoprecipitation and immunoblotting assays were performed with the indicated antibodies Data are representative of three independent experiments. (K) HEK293T cells were cotransfected with the plasmid encoding TBK1 and the plasmid encoding wild-type HBP21 or alanine mutant HBP21 upon VSV infection for 6 h. Immunoprecipitation and Western blotting were performed with the indicated antibodies. Data are representative of three independent experiments (means and SD in panels D and F).

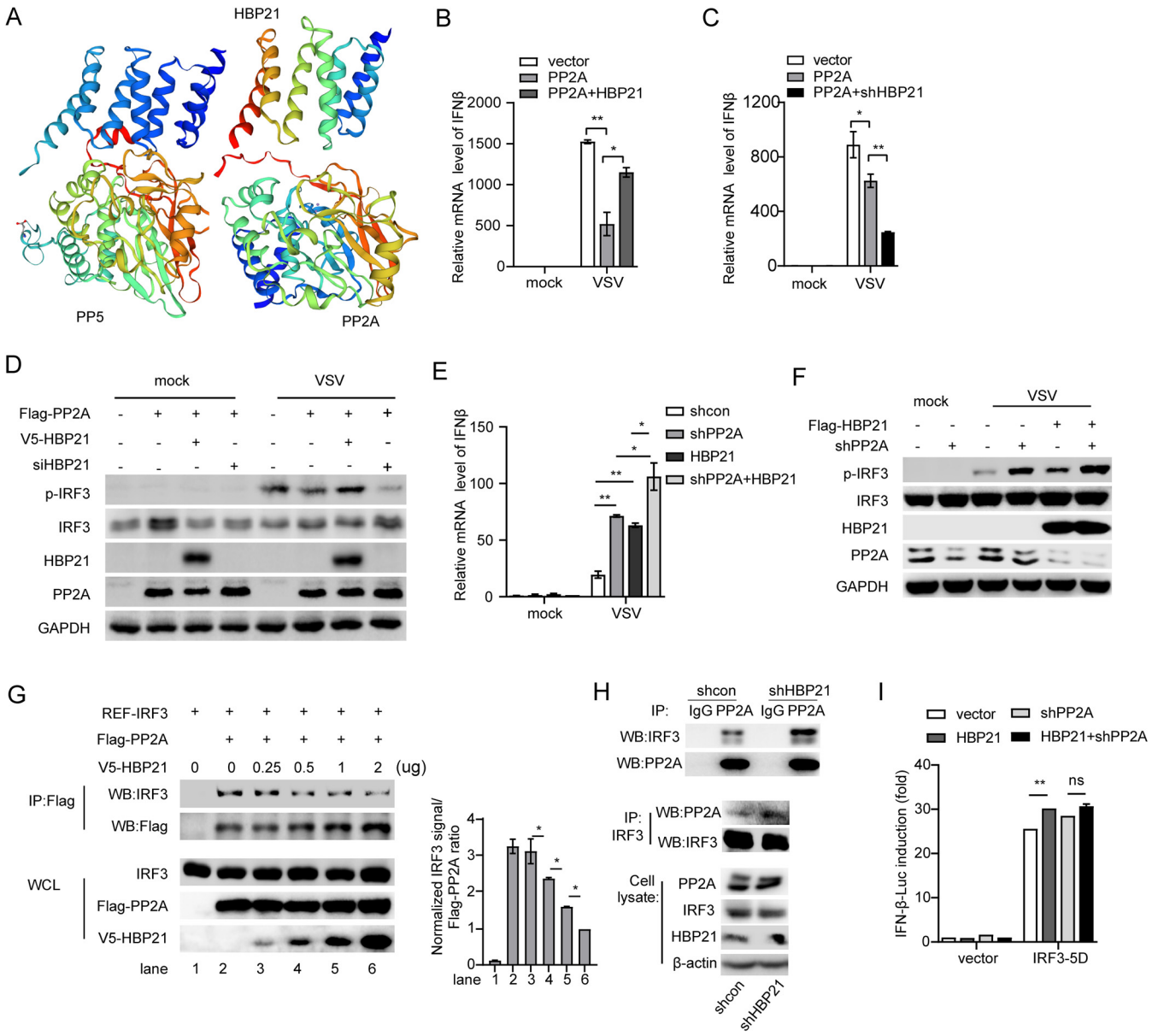

FIG 7 HBP21 blocks the interaction between PP2A and IRF3 to promote the innate immune response to viral infection. (A) The structure analysis of PP5, HBP21, and PP2A was predicted by the online software AlphaFold. (B to D) HLCZ01 cells were cotransfected with the plasmids encoding PP2A and HBP21 or shHBP21, followed by VSV infection for 9 h. IFN-β mRNA and phosphorylation of IRF3 at Ser396 were detected by real-time PCR and Western blotting, respectively. (E and F) HLCZ01 cells were infected with lenti-shPP2A or lenti-shVector and then transfected with the plasmid encoding HBP21, followed by VSV infection for 9 h. IFN-β mRNA and phosphorylation of IRF3 at Ser396 were detected by real-time PCR and Western blotting, respectively. (G) HEK293T cells were cotransfected with the indicated plasmids for 36 h. Immunoprecipitation and Western blotting were performed with the indicated antibodies. (H) HEK293T cells were infected by lenti-shHBP21 or lenti-shVector for 48 h. Immunoprecipitation and Western blotting were performed with the indicated antibodies. (I) Dual luciferase analysis of the activity of the IFN promoter in HEK293T cells infected by lenti-shPP2A or lenti-shVector for 48 h and cotransfected with pV5-HBP21, pIFN-luc, and p3XFlag-IRF3-5D or empty vector. Data are representative of three independent experiments (means and SD in panels B, C, E, and I).

the dephosphorylation of phosphatase PP2A of IRF3. Meanwhile, phosphorylated of HBP21 at S85 and S153 is important for the activation and formation of IRF3 dimerization. HBP21 promotes innate immunity and antiviral activity through different pathways. Our findings enhance our understanding of the novel immunological functions of molecular chaperones and provide new insights into the regulation of innate immunity.

DISCUSSION

HBP21, a chaperone of heat shock protein 70, interacts with HSP70, and plays an important role in tumor development. Our study shows that HBP21 promotes the innate immune

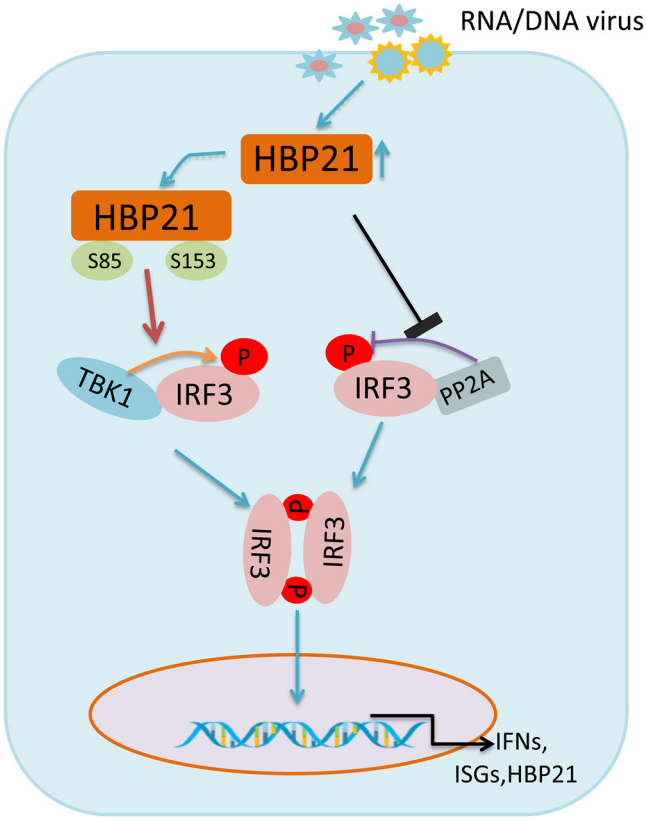

FIG 8 Schematic model of the dual regulation of IRF3 by HBP21. Upon virus infection, HBP21 is induced and phosphorylated at Ser85 and Ser153. The phosphorylated HBP21 at Ser85 and Ser153 enhances the formation of TBK1-IRF3 complex and triggers the phosphorylation of IRF3. Moreover, HBP21 promotes the activation of IRF3 by depressing the dephosphorylation of phosphatase PP2A of IRF3. HBP21 is important for IRF3 dimerization. HBP21 promotes innate immunity and antiviral activity through dual pathways.

response to viral infection. HSP70 is a protein used for synergistic immune action, which is a cytoprotective factor to protect cells from apoptosis induced by heat shock, serum starvation, or chemotherapeutic agents (45). HSP70 chaperones function in a wide range of cellular housekeeping activities, including the folding of newly synthesized proteins; the translocation of polypeptides into mitochondria, chloroplasts, and the ER; the disassembly of protein complexes; and the regulation of protein activity (46, 47). HBP21, as a molecular chaperone of HSP70, not only opens the door to innate immunity but also expands the function of HSP70 in immunity (21). Simultaneously, HBP21-regulated innate immunity is consistent with the idea that heat shock proteins can initiate innate immunity (48). Additionally, HSP70 and HBP21 are mostly distributed in the liver and heart. Our study demonstrates a previously unknown function for HBP21 associated with host defense against pathogen invasion.

As a tumor suppressor, HBP21 plays an important role in the regulation of innate immunity. HBP21 promotes virus-triggered activation of IRF3, the master controller of the production of IFNs. In the RLR-induced IRF3-mediated pathway of apoptosis (RIPA), IRF3 binds to the proapoptotic protein Bax and promotes apoptosis. HBP21 inhibits the interaction between HSP70 and Bax, promotes Bax protein translocation from cytoplasm to mitochondria, and finally induces apoptosis. Taken together, these observations indicate that HBP21 may provide a new and direct link between tumor suppression and antiviral pathway.

The phosphorylation-dependent role of HBP21 in the induction of IFN indicates that the existence of a potential kinase of HBP21 may be involved in innate immunity. So, in addition to the classic kinases such as IKKε and TBK1, other kinases may play an

important role in the activation of IRF3. Also, the unknown kinase phosphorylates Ser85 or Ser153 of HBP21 to regulate the phosphorylation of IRF3.

TPR can act as interaction scaffolds in the formation of protein-protein complexes involved in numerous cellular functions, such as transcription, protein translocation, and degradation. Virus-induced phosphorylation of HBP21 at Ser85 and Ser153 plays a critical role in the TBK1-IRF3 complex, which explains why HBP21's phosphorylation is important for the activation of IRF3. The TPR domain of HBP21 contains Ser85 and Ser153 of HBP21. As is well known from minute mutations in coding genes, such as point mutations or individual amino acid deletions, the encoded protein also has most of the biological activity, but the very subtle folding abnormalities of the protein product can lead to the occurrence of diseases. HBP21 is a highly conserved tumor suppressor gene, and its mutation may be related to the occurrence of tumors.

HBP21 impairs the ability of PP2A to block the activation of phosphorylated IRF3. According to the protein structure analysis, the structure of PP5 is like a recombinant protein composed of HBP21 and PP2A. Examination of the PP5 internal protein structure indicates that Glu76 of TPR-2 interacts with Arg275 and Tyr451 at the catalytic site. HBP21 possesses the TPR structure, and PP2A has the catalytic domain of PP5. However, interaction between HBP21 and PP2A could not be detected. PP5 has an α-J helix composed of several amino acids, which involves interaction between TPR and the catalytic domain (49). Perhaps for this reason, HBP21 and PP2A cannot interact with each other, or some intermediate proteins are required to participate. We did not test the effect of HBP21 on PP2A activity, which is a shortcoming of this study. It is reported that HBP21 blocks the interaction between HSP70 and Bax and enhances the release of cytochrome *c* (44). Our study supports the idea that HBP21 inhibits the ability of PP2A to block the activation of IRF3. The two mechanisms of HBP21 are functionally identical. These molecular mechanisms of HBP21 in regulating protein-protein complexes may provide a new and deeper understanding.

Chaperones perform the most basic physiological functions in cells, which means that they may be involved in the occurrence of many diseases and in maintaining physiological balance. The molecular chaperone cpn60 inhibits insulin-dependent diabetes and rheumatism in animal models. Molecular chaperones such as early pregnancy factors (EPF) in cpn10 have immunosuppressive effects, so they may play important roles during early embryonal development. (50, 51). In previous study, HBP21 inhibited the activation of AKT, which predicts the regulation of insulin resistance (52). Molecular chaperones can become immunodominant antigens in infectious diseases, stimulating the humoral immune response in the host and the cellular immune response mediated by T cells. HSP70 binds pathogen proteins (such as LPS, flagellin, and other lipid-based TLR ligands) or activates DC cells to escape pathogen contamination (53). HBP21 may be used as a vaccine to fight microbial infections and to treat tumors.

Overall, we propose that HBP21 as a chaperone may exert antitumor activity in part through the promotion of IFN responses, and thus, we have expanded HBP21's repertoire as a tumor suppressor. Our findings reveal HBP21's effect on antiviral immunity and may benefit the development of efficient therapeutic interventions for viral infection, human cancer, and numerous other diseases.

MATERIALS AND METHODS

Ethics statement. All animal experiments were carried out under the supervision of the Institutional Animal Care and Use Committee of Hunan University.

Mice. HBP21 knockout mice were established by CRISPR-Cas9-mediated genome editing on a C57BL/6J background. Briefly, a mixture of plasmids encoding Cas9 and single guide RNAs containing HBP21-1 (targeting site 1: GCCCCCCAGACATCATTATT) and HBP21-2 (targeting site 2: TGCCTAATAA TGATGTCTGG) were injected into fertilized ova. This technique was completed by Nanjing GemPharmatech Co., Ltd. The transgenic fertilized ova were implanted into pseudopregnant mice. For analysis of the genotype of each mouse, genomic DNA was removed from tail tissue clipped from F_1 and F_2 offspring and was assessed by PCR with the primers F1 (GTCATTCAGTCCCATACCTCTAAGCC), R1 (GTTTGTCACTCCTGGATCT CGG), F2 (CTTCTCTTAGCCAAGGAGAACCAC), and R2 (TCTTCTGTGGAGGATCTCTGG). We maintained all mice under specific-pathogen-free conditions and used 7- to 8-week-old mice in all experiments.

Reagents. Monoclonal antibodies against β-actin, Flag tag, and HA tag were obtained from Sigma. GAPDH antibody (MAB374) was purchased from Millipore. The V5 tag monoclonal antibody was from Invitrogen. The monoclonal antibody against HBP21 was purchased from Abcam. The antibodies for p-TBK1 (5483S), TBK1 (38066S), phosphorylated-IRF3 (S396) (4947S), IRF3 (4302S), phosphorylated-p65 (3033S), p65 (8242S), STING (13647S), LMNB1 (17416S), STAT1 (14994S), phosphorylated-STAT1 (9167S), STAT2 (72604S), and phosphorylated-STAT2 (88410S) and the horseradish peroxidase (HRP)-conjugated secondary antibody goat anti-rabbit IgG were purchased from Cell Signaling Technology. Rabbit polyclonal antibodies to IRF3 (11312-1-AP) and cGAS (26416-1-AP) were from Proteintech. Mouse monoclonal anti-HCV NS3 antibody was a gift from Chen Liu (Yale University). Goat anti-mouse IgG-HRP secondary antibody was obtained from Merck.

Cells and viruses. The HLCZ01 cell line, a novel hepatoma cell line supporting the entire life cycle of HCV and HBV, was previously established in our laboratory (28). HEK293T cells were purchased from Boster. HLCZ01 cells were cultured in collagen-coated tissue culture plates containing Dulbecco's modified Eagle's medium (DMEM)/F-12 medium supplemented with 10% (vol/vol) fetal bovine serum (FBS) (Gibco, 10270-106), 40 ng/mL of dexamethasone (Sigma), insulin-transferrin-selenium (ITS; Gibco, 41400-045), penicillin, and streptomycin. Other cells were propagated in DMEM supplemented with 10% FBS, L-glutamine, nonessential amino acids, penicillin, and streptomycin (29). To obtain mouse primary peritoneal macrophages, mice (male or female, 6 to 8 weeks old) were injected intraperitoneally with 3% fluid thioglycolate medium (Merck) (14). pJFH1 was a gift from Takaji Wakita (National Institute of Infectious Diseases, Tokyo, Japan). VSV and HSV were kindly shared by Xuetao Cao (Second Military Medical University, Shanghai, China). VSV-GFP and HSV-GFP were kindly shared by Hongbing Shu (Wuhan University, Wuhan, China).

Plasmid construction. The short hairpin RNA (shRNA) targeting HBP21 was inserted into the vector. The target sequence of HBP21 shRNA was GGCCATCTTCAACCCTGAC for lenti-shHBP21. MAVS was synthesized from the total cellular RNA isolated from HLCZ01 cells with the high-fidelity PCR kit KOD Plus-Neo (KOD-401; Toyobo, Tokyo, Japan). Subsequently, it was cloned into the pcDNA3.1a vector and the p3XFLAG-CMV vector. Multiple domains of HBP21 and IRF3 were amplified from the templates of full-length HBP21 and IRF3 and then cloned into the p3XFLAG-CMV or pcDNA3.1a vector. The HBP21 primers were assessed by PCR for amplifying genes with the forward primer CGGGGTACCATGGGGAC TCCAAATGATCA and reverse primer GCTCTAGAGCGGCTGTCACGGGGGCGGC. The target sequence of PP2A shRNA was GACGAGTGTTTAAGGAAAT for lenti-shPP2A. The IFN-luciferase plasmid was purchased from InvivoGen. The pLKO.1-shHBP21 plasmid was a gift from Xinyuan Guan (University of Hong Kong, Hong Kong, China). The Flag-IRF3-5D plasmid was a gift from Deyin Guo (Wuhan University, Wuhan, China). The plasmids Flag-TBK1 and pHA-Ub K63 were kindly provided by Zhengfan Jiang (Peking University, Beijing, China). The Flag-PP2A and Myc-MAVS were reported in our previous study (20, 29). Flag-cGAS and Flag-STING were kindly provided by Chen Wang (China Pharmaceutical University, Beijing, China).

Real-time PCR assay. Total cellular RNA was extracted by using the TRIzol reagent (Invitrogen, Carlsbad, CA) according to the manufacturer's protocol. A kit for reverse RNA transcription to cDNA was purchased from TaKaRa. Real-time PCR was performed as described previously (30). The primers for HBP21, IFN-β, IL-28A, VSV, HSV, GAPDH, ISG12a, GAPDH-mouse, and IFN-β-mouse were as follows: IFN-β-h-forward, CAGCATTTTCAGTGT CAGAAGC-3′; IFN-β-h-reverse, 5′-TCATCCTGTCCTTGAGGCAGT-3′; IL-28A-forward, 5′-GCCTCAGAGTTTCTTCT GC-3′; IL-28A reverse, 5′-AAGGCATCTTTGGCCCTCTT-3′; GAPDH forward, 5′-AATGGGCAGCCGTTAGGAAA-3′ GAPDH reverse, 5′-GCGCCCAATACGACCAAATC-3′; ISG12a forward, 5′-TGCCATGGGCTTCACTGCGG-3′; ISG12a reverse, 5′-CTGCCCGAGGCAACTCCACC-3′; HBP21 forward, 5′-CTTCAACCCTGACACCCCAT-3′; HBP21 reverse, 5′-GAGGGAAAACTTCATCTTCTTCTCG-3′; VSV forward, 5′-CAAGTCAAAATGCCCAAGAGTCACA-3′; VSV reverse, 5′-TTTCCTTGCATTGTTCTACAGATGG-3′; GAPDH-mouse forward 5′-CAGGAGAGTGTTTCCTCGTCC-3′; GAPDH-mouse reverse, 5′-TTCCCATTCTCGGCCTTGAC-3′; IFN-β-mouse forward, 5′-CGTGGGAGATGTCCTCAACT-3′; IFN-β-mouse reverse, 5′-AGATCTCTGCTCGGACCACC-3′; HSV PCR forward, 5′-GTGGTCCTGTGGAGCCTGTTG-3′; HSV PCR reverse, 5′-GGGTGGTGTTGTTCTTGGGTTT-3′.

Luciferase assay. Luciferase reporter assays were performed with a luciferase assay kit (Promega). Luciferase activity was measured according to the manufacturer's protocol.

DNA extraction. Genomic DNA extraction from mice or cells was performed with a DNA assay kit (Tiangen) according to the manufacturer's instructions.

Nuclear and cytoplasmic extraction. Cells were washed once with phosphate-buffered saline (PBS) and lysed in lysis buffer A (150 mM KCl, 25 mM Tris-HCl [pH 7.5], 5 mM EDTA, 1% Triton X-100, 2 mM dithiothreitol [DTT]) supplemented with a protease inhibitor cocktail. The cell lysates were incubated on ice for 15 min and centrifuged at 1,000 × *g* at 4°C for 5 min. The supernatant was cytoplasmic, and the sediment was washed 3 times with ice-cold PBS. The sediment was lysed in lysis buffer B (500 mM KCl, 25 mM Tris-HCl [pH 7.5], 2 mM EDTA, 1% NP-40, 1% SDS) for 30 min. Nuclear and cytoplasmic lysates were cleared by centrifugation at 16,000 × *g* for 10 min.

H&E staining. For hematoxylin and eosin (H&E) staining, tissue samples were routinely embedded in paraffin, followed by slicing and dewaxing. The slices were stained with hematoxylin (Boster, Wuhan, China) for 15 min, rinsed with water, dehydrated with alcohol, and counterstained with eosin (Boster) for 5 min (54). Images were obtained using the Pannoramic MIDI II tissue biopsy scan system (3DHISTECH Ltd., Budapest, Hungary).

Coimmunoprecipitation (co-IP), immunoblot analysis, and native PAGE. Cells were washed with PBS and lysed with lysis buffer (Thermo Scientific, 87787) containing protease inhibitors. The cell lysates were incubated on ice for 25 min and centrifuged at 16,000 × *g* at 4°C for 15 min. Then, 400 × *g* of protein in PBS was immunoprecipitated with the indicated antibodies overnight. The immunocomplex was captured by adding a protein G-agarose bead slurry for 6 h. The protein binding to the beads was boiled in 2× Laemmli sample buffer at 100°C for 5 min and then subjected to immunoblot analysis. Native PAGE was performed with a 10% acrylamide gel without SDS. The gel was prerun for 30 min at 40 mA

on ice with 25 mM Tris-HCl (pH 8.4) and 192 mM glycine with or without 1% deoxycholate in the cathode chamber and anode chamber, respectively. Samples in the 5× native sample buffer (312.5 mM Tris-HCl [pH 6.8], 75% glycerol, 0.25% bromophenol blue) were applied on the gel and underwent electrophoresis for 60 min at 25 mA on ice, followed by immunoblot analysis.

Lentiviral gene transfer. HEK293T cells (5×10^6) were transfected with the appropriate lentiviral expression plasmid (8 μg) together with the empty vector along with the packaging vectors pSPAX2 (8 μg) and pMD2G (2.7 μg) in a 10-cm dish after 24h transfection. The virus-rich supernatant was harvested and then used for infection of cells. The infection was repeated twice to enhance the transduction efficiency.

Phos-tag analysis. Cells were washed with PBS and lysed in lysis buffer (Thermo Scientific, 89900) containing protease inhibitors. One part protein was added Lambda Protein phosphatase (New England Biolabs, P0753S) according to the manufacturer's instructions (55). Reactions were stopped by adding an equal volume of 2× sample buffer and boiling for 5 min. Samples were then separated by 12% SDS–PAGE contained 100 μM Phos-binding reagent acrylamide (APExBIO, F4002) and 200 μM $MnCl_2$ for 80 min. The SDS-PAGE gel was washed by EDTA buffer, and then samples were transferred onto polyvinylidene difluoride (PVDF) membranes for immunoblotting analyses (56). Phos-tag analysis was performed according to the manufacturer's instructions.

Virus plaque assay. Supernatants from HEK293T cells were harvested and diluted at $1:10^1$ to $1:10^9$. The diluted virus was used to infect Huh7 cells. One hour after infection, the supernatants were removed and the new medium containing 1% agar was overlaid on the cells. At 2 days after infection, the cells were fixed for 20 min with 4% formaldehyde and then stained with 0.2% crystal violet. Plaques were counted. The results were averaged and multiplied by the dilution factor for the calculation of viral titers as PFU/mL.

Statistical analysis. All experiments were replicated at least two times, and the data from parallel cultures were acquired. The significance of the difference between the control and experimental groups was tested using Student's *t* test. The statistical significance of survival curves was estimated according to the method of Kaplan and Meier. Differences were considered significant when P was <0.05. Data were analyzed with GraphPad Prism software.

ACKNOWLEDGMENTS

We acknowledge Charles M. Rice (Rockefeller University, New York) for Huh7.5 cells to prepare for HCV. We thank Takaji Wakita for pJFH1 plasmid (National Institute of Infectious Diseases, Tokyo). We thank Chen Liu (Yale University), Hongbing Shu (Wuhan University), Jianguo Wu (Wuhan University), Zhengfan Jiang (Peking University), Deyin Guo (Wuhan University), Chen Wang, and Xinyuan Guan (The University of Hong Kong) kindly sharing research materials.

This work was supported by the National Natural Science Foundation of China (81730064, 81902069, 82072269, and 81571985), National Science and Technology Major Project (2017ZX10202201), and Hunan Natural Science Foundation (2018JJ3090).

REFERENCES

1. Fensterl V, Chattopadhyay S, Sen GC. 2015. No love lost between viruses and interferons. Annu Rev Virol 2:549–572. https://doi.org/10.1146/annurev-virology-100114-055249.
2. Chattopadhyay S, Sen GC. 2017. RIG-I-like receptor-induced IRF3 mediated pathway of apoptosis (RIPA): a new antiviral pathway. Protein Cell 8:165–168. https://doi.org/10.1007/s13238-016-0334-x.
3. Loo YM, Gale M, Jr. 2011. Immune signaling by RIG-I-like receptors. Immunity 34:680–692. https://doi.org/10.1016/j.immuni.2011.05.003.
4. King KR, Aguirre AD, Ye YX, Sun Y, Roh JD, Ng RP, Jr, Kohler RH, Arlauckas SP, Iwamoto Y, Savol A, Sadreyev RI, Kelly M, Fitzgibbons TP, Fitzgerald KA, Mitchison T, Libby P, Nahrendorf M, Weissleder R. 2017. IRF3 and type I interferons fuel a fatal response to myocardial infarction. Nat Med 23:1481–1487. https://doi.org/10.1038/nm.4428.
5. Mino T, Takeuchi O. 2017. NSD3 keeps IRF3 active. J Exp Med 214:3475–3476. https://doi.org/10.1084/jem.20171980.
6. Sato M, Suemori H, Hata N, Asagiri M, Ogasawara K, Nakao K, Nakaya T, Katsuki M, Noguchi S, Tanaka N, Taniguchi T. 2000. Distinct and important roles of transcription factors IRF-3 and IRF-7 in response to viruses for IFN-alpha/beta gene induction. Immunity 13:539–548. https://doi.org/10.1016/S1074-7613(00)00053-4.
7. Yang Q, Shu HB. 2020. Deciphering the pathways to antiviral innate immunity and inflammation. Adv Immunol 145:1–36. https://doi.org/10.1016/bs.ai.2019.11.001.
8. Lu B, Ren Y, Sun X, Han C, Wang H, Chen Y, Peng Q, Cheng Y, Cheng X, Zhu Q, Li W, Li HL, Du HN, Zhong B, Huang Z. 2017. Induction of INKIT by viral infection negatively regulates antiviral responses through inhibiting phosphorylation of p65 and IRF3. Cell Host Microbe 22:86–98.E4. https://doi.org/10.1016/j.chom.2017.06.013.
9. McNab F, Mayer-Barber K, Sher A, Wack A, O'Garra A. 2015. Type I interferons in infectious disease. Nat Rev Immunol 15:87–103. https://doi.org/10.1038/nri3787.
10. Hubel P, Urban C, Bergant V, Schneider WM, Knauer B, Stukalov A, Scaturro P, Mann A, Brunotte L, Hoffmann HH, Schoggins JW, Schwemmle M, Mann M, Rice CM, Pichlmair A. 2019. A protein-interaction network of interferon-stimulated genes extends the innate immune system landscape. Nat Immunol 20:493–502. https://doi.org/10.1038/s41590-019-0323-3.
11. Zhang Q, Cao X. 2019. Epigenetic regulation of the innate immune response to infection. Nat Rev Immunol 19:417–432. https://doi.org/10.1038/s41577-019-0151-6.
12. Lazear HM, Schoggins JW, Diamond MS. 2019. Shared and distinct functions of type I and type III interferons. Immunity 50:907–923. https://doi.org/10.1016/j.immuni.2019.03.025.
13. Schoggins JW, Wilson SJ, Panis M, Murphy MY, Jones CT, Bieniasz P, Rice CM. 2011. A diverse range of gene products are effectors of the type I interferon antiviral response. Nature 472:481–485. https://doi.org/10.1038/nature09907.
14. Huai W, Liu X, Wang C, Zhang Y, Chen X, Chen X, Xu S, Thomas T, Li N, Cao X. 2019. KAT8 selectively inhibits antiviral immunity by acetylating IRF3. J Exp Med 216:772–785. https://doi.org/10.1084/jem.20181773.
15. Chen W, Srinath H, Lam SS, Schiffer CA, Royer WE, Jr, Lin K. 2008. Contribution of Ser386 and Ser396 to activation of interferon regulatory factor 3. J Mol Biol 379:251–260. https://doi.org/10.1016/j.jmb.2008.03.050.

16. Hu MM, Shu HB. 2018. Cytoplasmic mechanisms of recognition and defense of microbial nucleic acids. Annu Rev Cell Dev Biol 34:357–379. https://doi.org/10.1146/annurev-cellbio-100617-062903.
17. Fitzgerald KA, McWhirter SM, Faia KL, Rowe DC, Latz E, Golenbock DT, Coyle AJ, Liao SM, Maniatis T. 2003. IKKepsilon and TBK1 are important components of the IRF3 signaling pathway. Nat Immunol 4:491–496. https://doi.org/10.1038/ni921.
18. Liu S, Cai X, Wu J, Cong Q, Chen X, Li T, Du F, Ren J, Wu YT, Grishin NV, Chen ZJ. 2015. Phosphorylation of innate immune adaptor proteins MAVS, STING, and TRIF induces IRF3 activation. Science 347:aaa2630. https://doi.org/10.1126/science.aaa2630.
19. Zhang H, Han C, Li T, Li N, Cao X. 2019. The methyltransferase PRMT6 attenuates antiviral innate immunity by blocking TBK1-IRF3 signaling. Cell Mol Immunol 16:800–809. https://doi.org/10.1038/s41423-018-0057-4.
20. Wang J, Li H, Xue B, Deng R, Huang X, Xu Y, Chen S, Tian R, Wang X, Xun Z, Sang M, Zhu H. 2020. IRF1 promotes the innate immune response to viral infection by enhancing the activation of IRF3. J Virol 94:e01231-20. https://doi.org/10.1128/JVI.01231-20.
21. Liu Q, Gao J, Chen X, Chen Y, Chen J, Wang S, Liu J, Liu X, Li J. 2008. HBP21: a novel member of TPR motif family, as a potential chaperone of heat shock protein 70 in proliferative vitreoretinopathy (PVR) and breast cancer. Mol Biotechnol 40:231–240. https://doi.org/10.1007/s12033-008-9080-5.
22. Carrello A, Allan RK, Morgan SL, Owen BA, Mok D, Ward BK, Minchin RF, Toft DO, Ratajczak T. 2004. Interaction of the Hsp90 cochaperone cyclophilin 40 with Hsc70. Cell Stress Chaperones 9:167–181. https://doi.org/10.1379/csc-26r.1.
23. Cerveny L, Straskova A, Dankova V, Hartlova A, Ceckova M, Staud F, Stulik J. 2013. Tetratricopeptide repeat motifs in the world of bacterial pathogens: role in virulence mechanisms. Infect Immun 81:629–635. https://doi.org/10.1128/IAI.01035-12.
24. Zeytuni N, Zarivach R. 2012. Structural and functional discussion of the tetra-trico-peptide repeat, a protein interaction module. Structure 20:397–405. https://doi.org/10.1016/j.str.2012.01.006.
25. Zhou Y, He Q, Chen J, Liu Y, Mao Z, Lyu Z, Ni D, Long Y, Ju P, Liu J, Gu Y, Zhou Q. 2016. The expression patterns of Tetratricopeptide repeat domain 36 (Ttc36). Gene Expr Patterns 22:37–45. https://doi.org/10.1016/j.gep.2016.11.001.
26. Xu Y, Cao J, Huang S, Feng D, Zhang W, Zhu X, Yan X. 2015. Characterization of tetratricopeptide repeat-containing proteins critical for cilia formation and function. PLoS One 10:e0124378. https://doi.org/10.1371/journal.pone.0124378.
27. Sunryd JC, Cheon B, Graham JB, Giorda KM, Fissore RA, Hebert DN. 2014. TMTC1 and TMTC2 are novel endoplasmic reticulum tetratricopeptide repeat-containing adapter proteins involved in calcium homeostasis. J Biol Chem 289:16085–16099. https://doi.org/10.1074/jbc.M114.554071.
28. Yang D, Zuo C, Wang X, Meng X, Xue B, Liu N, Yu R, Qin Y, Gao Y, Wang Q, Hu J, Wang L, Zhou Z, Liu B, Tan D, Guan Y, Zhu H. 2014. Complete replication of hepatitis B virus and hepatitis C virus in a newly developed hepatoma cell line. Proc Natl Acad Sci U S A 111:E1264–E1273. https://doi.org/10.1073/pnas.1320071111.
29. Xue B, Li H, Guo M, Wang J, Xu Y, Zou X, Deng R, Li G, Zhu H. 2018. TRIM21 promotes innate immune response to RNA viral infection through Lys27-linked polyubiquitination of MAVS. J Virol 92:e00321-18. https://doi.org/10.1128/JVI.00321-18.
30. Xie Q, Chen S, Tian R, Huang X, Deng R, Xue B, Qin Y, Xu Y, Wang J, Guo M, Chen J, Tang S, Li G, Zhu H. 2018. Long noncoding RNA ITPRIP-1 positively regulates the innate immune response through promotion of oligomerization and activation of MDA5. J Virol 92:e00507-18. https://doi.org/10.1128/JVI.00507-18.
31. Xue B, Yang D, Wang J, Xu Y, Wang X, Qin Y, Tian R, Chen S, Xie Q, Liu N, Zhu H. 2016. ISG12a restricts hepatitis C virus infection through the ubiquitination-dependent degradation pathway. J Virol 90:6832–6845. https://doi.org/10.1128/JVI.00352-16.
32. Carlin AF, Plummer EM, Vizcarra EA, Sheets N, Joo Y, Tang W, Day J, Greenbaum J, Glass CK, Diamond MS, Shresta S. 2017. An IRF-3-, IRF-5-, and IRF-7-independent pathway of dengue viral resistance utilizes IRF-1 to stimulate type I and II interferon responses. Cell Rep 21:1600–1612. https://doi.org/10.1016/j.celrep.2017.10.054.
33. Yang D, Meng X, Xue B, Liu N, Wang X, Zhu H. 2014. MiR-942 mediates hepatitis C virus-induced apoptosis via regulation of ISG12a. PLoS One 9:e94501. https://doi.org/10.1371/journal.pone.0094501.
34. Lin R, Heylbroeck C, Pitha PM, Hiscott J. 1998. Virus-dependent phosphorylation of the IRF-3 transcription factor regulates nuclear translocation, transactivation potential, and proteasome-mediated degradation. Mol Cell Biol 18:2986–2996. https://doi.org/10.1128/MCB.18.5.2986.
35. Zhu Z, Li P, Yang F, Cao W, Zhang X, Dang W, Ma X, Tian H, Zhang K, Zhang M, Xue Q, Liu X, Zheng H. 2019. Peste des petits ruminants virus nucleocapsid protein inhibits beta interferon production by interacting with IRF3 to block its activation. J Virol 93:e00362-19. https://doi.org/10.1128/JVI.00362-19.
36. Fitzgerald KA, Kagan JC. 2020. Toll-like receptors and the control of immunity. Cell 180:1044–1066. https://doi.org/10.1016/j.cell.2020.02.041.
37. Sanchez-deAlcazar D, Mejias SH, Erazo K, Sot B, Cortajarena AL. 2018. Self-assembly of repeat proteins: concepts and design of new interfaces. J Struct Biol 201:118–129. https://doi.org/10.1016/j.jsb.2017.09.002.
38. Ramsey AJ, Russell LC, Chinkers M. 2009. C-terminal sequences of hsp70 and hsp90 as non-specific anchors for tetratricopeptide repeat (TPR) proteins. Biochem J 423:411–419. https://doi.org/10.1042/BJ20090543.
39. Sumanasekera WK, Tien ES, Davis JW, II, Turpey R, Perdew GH, Vanden Heuvel JP. 2003. Heat shock protein-90 (Hsp90) acts as a repressor of peroxisome proliferator-activated receptor-alpha (PPARalpha) and PPARbeta activity. Biochemistry 42:10726–10735. https://doi.org/10.1021/bi0347353.
40. Yang J, Roe SM, Cliff MJ, Williams MA, Ladbury JE, Cohen PT, Barford D. 2005. Molecular basis for TPR domain-mediated regulation of protein phosphatase 5. EMBO J 24:1–10. https://doi.org/10.1038/sj.emboj.7600496.
41. Long L, Deng Y, Yao F, Guan D, Feng Y, Jiang H, Li X, Hu P, Lu X, Wang H, Li J, Gao X, Xie D. 2014. Recruitment of phosphatase PP2A by RACK1 adaptor protein deactivates transcription factor IRF3 and limits type I interferon signaling. Immunity 40:515–529. https://doi.org/10.1016/j.immuni.2014.01.015.
42. Senior AW, Evans R, Jumper J, Kirkpatrick J, Sifre L, Green T, Qin C, Zidek A, Nelson AWR, Bridgland A, Penedones H, Petersen S, Simonyan K, Crossan S, Kohli P, Jones DT, Silver D, Kavukcuoglu K, Hassabis D. 2020. Improved protein structure prediction using potentials from deep learning. Nature 577:706–710. https://doi.org/10.1038/s41586-019-1923-7.
43. Shi Y. 2009. Serine/threonine phosphatases: mechanism through structure. Cell 139:468–484. https://doi.org/10.1016/j.cell.2009.10.006.
44. Jiang L, Kwong DL, Li Y, Liu M, Yuan YF, Li Y, Fu L, Guan XY. 2015. HBP21, a chaperone of heat shock protein 70, functions as a tumor suppressor in hepatocellular carcinoma. Carcinogenesis 36:1111–1120. https://doi.org/10.1093/carcin/bgv116.
45. Tao J, Berthet A, Citron YR, Tsiolaki PL, Stanley R, Gestwicki JE, Agard DA, McConlogue L. 2021. Hsp70 chaperone blocks alpha-synuclein oligomer formation via a novel engagement mechanism. J Biol Chem 296:100613. https://doi.org/10.1016/j.jbc.2021.100613.
46. Bailly AP, Perrin A, Serrano-Macia M, Maghames C, Leidecker O, Trauchessec H, Martinez-Chantar ML, Gartner A, Xirodimas DP. 2019. The balance between mono- and NEDD8-chains controlled by NEDP1 upon DNA damage is a regulatory module of the HSP70 ATPase activity. Cell Rep 29:212–224.E8. https://doi.org/10.1016/j.celrep.2019.08.070.
47. Brykczynska U, Geigges M, Wiedemann SJ, Dror E, Boni-Schnetzler M, Hess C, Donath MY, Paro R. 2020. Distinct transcriptional responses across tissue-resident macrophages to short-term and long-term metabolic challenge. Cell Rep 30:1627–1643.E7. https://doi.org/10.1016/j.celrep.2020.01.005.
48. Tsan MF, Gao B. 2009. Heat shock proteins and immune system. J Leukoc Biol 85:905–910. https://doi.org/10.1189/jlb.0109005.
49. Oberoi J, Dunn DM, Woodford MR, Mariotti L, Schulman J, Bourboulia D, Mollapour M, Vaughan CK. 2016. Structural and functional basis of protein phosphatase 5 substrate specificity. Proc Natl Acad Sci U S A 113:9009–9014. https://doi.org/10.1073/pnas.1603059113.
50. McCombe PA. 2008. Recombinant EPF/chaperonin 10 promotes the survival of O4-positive pro-oligodendrocytes prepared from neonatal rat brain. Cell Stress Chaperones 13:467–474. https://doi.org/10.1007/s12192-008-0045-1.
51. Kawamura K, Fukuda J, Itoh H, Ito K, Kodama H, Kumagai J, Kumagai A, Tanaka T. 2000. Chaperonin 10 in the rat oocytes and early embryos: its expression and activity for early pregnancy factor. Am J Reprod Immunol 44:242–248. https://doi.org/10.1111/j.8755-8920.2000.440409.x.
52. Song L, Guo X, Zhao F, Wang W, Zhao Z, Jin L, Wu C, Yao J, Ma Z. 2021. TTC36 inactivation induce malignant properties via Wnt-beta-catenin

pathway in gastric carcinoma. J Cancer 12:2598–2609. https://doi.org/10.7150/jca.47292.
53. Chen T, Cao X. 2010. Stress for maintaining memory: HSP70 as a mobile messenger for innate and adaptive immunity. Eur J Immunol 40:1541–1544. https://doi.org/10.1002/eji.201040616.
54. Deng R, Zuo C, Li Y, Xue B, Xun Z, Guo Y, Wang X, Xu Y, Tian R, Chen S, Liu Q, Chen J, Wang J, Huang X, Li H, Guo M, Wang X, Yang M, Wu Z, Wang J, Ma J, Hu J, Li G, Tang S, Tu Z, Ji H, Zhu H. 2020. The innate immune effector ISG12a promotes cancer immunity by suppressing the canonical Wnt/beta-catenin signaling pathway. Cell Mol Immunol 17:1163–1179. https://doi.org/10.1038/s41423-020-00549-9.
55. Xie Y, Lv X, Ni D, Liu J, Hu Y, Liu Y, Liu Y, Liu R, Zhao H, Lu Z, Zhou Q. 2019. HPD degradation regulated by the TTC36-STK33-PELI1 signaling axis induces tyrosinemia and neurological damage. Nat Commun 10:4266. https://doi.org/10.1038/s41467-019-12011-0.
56. Kinoshita E, Kinoshita-Kikuta E, Koike T. 2009. Separation and detection of large phosphoproteins using Phos-tag SDS-PAGE. Nat Protoc 4:1513–1521. https://doi.org/10.1038/nprot.2009.154.